Optics Letters

Diode-side-pumped, intracavity Nd:YLF/KGW/LBO Raman laser at 573 nm for retinal photocoagulation

MERILYN S. FERREIRA AND NIKLAUS U. WETTER*

Lasers and Applications Center, Nuclear and Energy Research Institute, IPEN, LineuPrestes 2242, São Paulo 05508-000, Brazil
**Corresponding author: nuwetter@ipen.br*

Received 6 October 2020; revised 16 December 2020; accepted 17 December 2020; posted 18 December 2020 (Doc. ID 411895); published 21 January 2021

Wavelengths in the yellow-orange range are of significant interest for retinal photocoagulation and are especially important in the case of diabetic retinopathy, which can cause blindness and affects 3.3% of all working-age adults. This work presents a highly-efficient, compact, and cost-efficient side-pumped, intracavity Raman configuration to achieve this objective. A side-pumped Nd:YLF/KGW/LBO frequency-doubled Raman laser producing 11.7 W of output power at 1147 nm with 21% of slope efficiency and 6 W of output power at 573.5 nm with 12% slope efficiency is demonstrated.

https://doi.org/10.1364/OL.411895

Laser emission wavelengths in the yellow-orange range are of interest due to their large number of applications such as sodium laser guide star, medical and biomedical applications, display technology, and quantum computation [1,2]. For example, in fluorescence microscopy, 588 nm laser light is used because some fluorophores have their absorption peak at this wavelength, and in flow cytometry, there is a demand for laser wavelengths between 561 nm and 640 nm with stringent characteristics in terms of power stability, low noise, and Gaussian mode beam quality [3,4]. An important application is in the treatment of ophthalmologic diseases of the retina, where the orange-yellow radiation presents good clinical results with minimal collateral effects [5]. The most common eye disease causing vision impairment and blindness is diabetic retinopathy, which affects about 3.3% of all working-age adults and is treated by retinal laser photocoagulation [6].

The main components of the retina that are responsible for the photocoagulation process are hemoglobin, oxyhemoglobin, xanthophyll, and melanin. Absorption by hemoglobin, oxyhemoglobin, and melanin should be optimized to restrict absorption to the highly vascularized thin layer on top of the photoreceptors. The chromophore xanthophyll has high absorption at wavelengths below 550 nm, is abundant in the retinal macula, and occurs predominantly in regions that are not vascularized. Therefore, absorption below 550 nm should be minimized to avoid unnecessary pain and possibly damage to the eyesight. The other three chromophores have decreasing absorption for wavelengths longer than 576 nm, with oxyhemoglobin showing a strong and distinct peak at this wavelength and a sharp drop off at longer wavelengths, as seen by observing the absorption spectra for these three chromophores [7]. Therefore, using wavelengths beyond 576 nm causes deeper and more painful lesions. For these reasons, the ideal wavelength for photocoagulation is 576 nm and, when comparing with longer wavelengths, slightly smaller wavelengths should give better results.

Using the radiation proposed in this work, 573.5 nm, we hypothesized that higher treatment efficiency should be obtained when compared to lasers at 588 nm.

The first applications of retinal photocoagulation used traditional, inefficient, and costly dye lasers emitting at 576 nm. Later on, expensive vertical-cavity surface-emitting lasers (VCSELS), optical parametric oscillators (OPOs), and fiber lasers came to use, resulting ultimately in more cost-efficient Raman lasers. Today's yellow photocoagulators are generally based on the second harmonic generation (SHG) of near-IR emitting devices and, in this regard, Raman lasers present a series of characteristics that make these lasers the lasers of choice. These characteristics are typically compact in design, efficiency, and affordability with sufficiently good beam quality. Among the intracavity-converted Raman lasers, self-Raman lasers are the most efficient ones, showing typically a conversion efficiency of 10%–20% for the Raman wavelength and before SHG. Some self-Raman lasers have become commercial such as Nd:YVO_4 with intracavity SHG generating 588 nm with an output power of 7.9 W [8]. Separating the fundamental crystal from the Raman crystal is favorable for thermal management and decreases thermal lensing. Moreover, this separation allows for greater wavelength flexibility because a Raman crystal, showing Stokes shifts other than those of the fundamental crystal, can be used. This allows the laser to be tailored to the specific application.

The first work based on a neodymium-doped and diode-pumped intracavity Raman laser was reported in 2007, using a Nd:$GdVO_4$ crystal for the fundamental laser and a potassium gadolinium tungstate [$KGd(WO_4)_2$ or KGW] crystal for Stokes conversion to 1173 nm. In this work, 678 mW of output power at 586 nm was achieved with 4.1% optical efficiency

using lithium triborate (LiB_3O_5 or LBO) for SHG [9]. The same fundamental laser and a $BaWO_4$ Raman crystal achieved 2.51 W of output power at 586.5 nm with 12.2% of optical efficiency [10]. A self-Raman laser at 588 nm was reported with 8.4% of optical efficiency and output power of 320 mW using Nd:YVO_4 and LBO for SHG [11]. Another work reported that 3.5 W at 586 nm was obtained with a self-Raman laser using a Nd:$GdVO_4$ crystal [12]. Another work with good results achieved 3.5 W of yellow output power and 13.3% optical efficiency with a Nd:$LuVO_4$ self-Raman laser [13]. To our knowledge, the highest yellow output power at 588 nm of 7.9 W was reported using a Q-switched, Nd:YVO self-Raman laser using two diffusion bonded end-caps on the crystal [8].

Nd:$LiYF_4$ (Nd:YLF) shows several benefits when used as the fundamental laser crystal in intracavity Raman lasers. It offers a naturally polarized emission and a weak thermal lens when compared with isotropic crystals such as YAG [14]. Its π and σ polarized emissions show different wavelengths, 1047 nm and 1053 nm, respectively, which are shorter than the traditional oxide crystals (1064 nm), thus providing an unusual range of Stokes wavelengths and corresponding visible wavelengths. If a specific polarization is required (π or σ), the crystal facets can be wedged at the Brewster angle for polarization selection.

The first Nd:YLF Raman laser was developed by Savitski *et al.* and operated in the π polarization at 1047 nm to pump a diamond crystal, obtaining 5.1 W at 1217 nm [15]. The authors also pumped a KGW crystal with this same system, obtaining 6.1 W at 1139 nm, corresponding to a diode-to-Stokes conversion efficiency of 4%. Bu *et al.* operated a Nd:YLF based laser at 1047 nm that was Stokes shifted using a $SrWO_4$ crystal and then frequency doubled in LBO to generate a laser source at 579 nm with 889 mW output power; this corresponded to a diode-to-yellow conversion efficiency of 5.8% [16]. A more recent work, reported by Neto *et al.*, consisted of a Brewster-angled Nd:YLF/KGW Raman laser pumped in a longitudinal configuration in continuous-wave (cw) operation [17]. Their results can be directly compared to our results since they obtained, for the first time, the same wavelengths reported in this work. They achieved results for quasi-cw operation at near-IR and yellow wavelengths of 1.2 W output power at 1147 nm, with 6% of conversion efficiency with respect to absorbed pump power and 1.25 W of output power at 573 nm with 7% optical efficiency.

So far, all these works have used longitudinal diode pumping where the pump direction is parallel to the laser's optical axis. One of the benefits of the diode-side-pumped cavity setup is power scaling, which is difficult in a diode-end-pumped configuration because of two main challenges: the coupling of the pump beams to the optical axis of the laser resonator, and the heat management of the concentrated pump radiation that causes strong thermal lensing. Furthermore, increasing the power in fiber-coupled diode pump sources is typically accompanied by an exponential increase in system cost, a larger spectral bandwidth and absence of polarized pump radiation, which in turn decreases overall efficiency.

The previously mentioned drawbacks associated with the longitudinal pumping scheme may be avoided, without loss of efficiency, by using a side-pumped setup with Brewster angle incidence geometry combined with the total internal reflection (TIR) of the laser beam at the crystal's pump facet. Specifically in the case of Nd:YLF, it has been shown that this side-pumping technology is much more efficient (65%) than longitudinal pumping while maintaining fundamental mode beam quality [18].

The first intracavity-converted, diode-side-pumped Raman laser was reported by Kores *et al.* showing a Nd:YVO_4 self-Raman laser operating at 1176 nm with an optical conversion efficiency of 11.5% and 8 W of output power [19]. Here, we demonstrate for the first time, to our knowledge, a diode-side-pumped Nd:YLF_4/KGW Raman laser that generates 11.7 W of output power at 1147 nm with 21% of slope efficiency and 6 W of output power at 573.5 nm and 12% slope efficiency.

The Nd:$YLiF_4$ fundamental laser crystal with 1% doping (Crystech Inc.) was an a-cut quadratic slice (Fig. 1) of dimensions $13 \times 13 \times 3\ mm^3$ without anti-reflective coatings since the Brewster angle incidence (55.4°, refractive index of 1.45) of the resonant beam at the crystal facets (dimensions of facets: 13 mm × 3 mm) was chosen, thus selecting the σ polarization responsible for the 1053 nm emission. This allowed larger beam dimensions in the horizontal direction (aspect ratio of 1.3 for a Gaussian beam) for better overlap with the pump beam coming from the side. Additionally, the laser beam undergoes a TIR at the pump facet to achieve a good spatial overlap between the locus of highest inversion density inside the crystal with highest intensity cross section of the resonant beam. The pump source was a 120 W diode laser emitting at 797 nm (Northrop Grumman) and fitted with a volume Bragg grating (VBG) for emission linewidth narrowing (FWHM ~0.5 nm) in order to achieve better overlap with the crystal's absorption peak. It is important to notice that the primary objective of the diode's VBG is beam quality improvement. The improved overlap causes an increase of almost 40% in the absorption coefficient, which, in turn, decreases the pump beam penetration depth into the crystal, thereby improving greatly the fundamental beam's quality [18].

The diode was operated at a frequency of 5 Hz with a pulse width of 350 μs (FWHM). A half-wave plate (HWP) was used to align the polarization of the diode emission with the crystal's π polarization, which was perpendicular to the $13 \times 13\ mm^2$

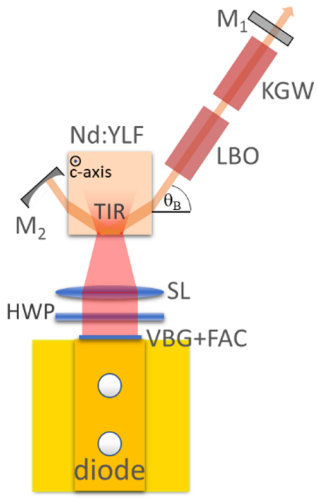

Fig. 1. Laser cavity setup containing a VBG and fast axis collimating (FAC)-equipped diode emitting at 797 nm, an HWP, and an f = 30 mm spherical lens (SL) for aligning the polarization and collimating the pump beam into the a-cut Nd:YLF crystal slab, a partial reflectivity mirror M_1, a high-reflectivity curved mirror M_2, a KGW Raman crystal, and a LBO SHG crystal. The resonant laser beam undergoes TIR at the crystal's pump facet.

facets. A bi-convex lens with 29 mm focal distance concentrated the pump beam into the laser crystal generating a line focus in the horizontal direction of approximately 3.5 mm × 0.2 mm at the crystal's pump facet. A KGW crystal (Castech Inc.) was chosen as the Raman laser crystal because it has a high Raman gain of ∼4.5 cm/GW, similar to the vanadates [20]. KGW has two strong Raman lines at 768 cm^{-1} and at 901 cm^{-1} of similar gain that can be accessed separately just by the orientation of the KGW with respect to the polarization of the fundamental beam, giving rise to emission at two different Stokes wavelengths of 1147 nm and 1163 nm, respectively. In this work, we are interested in the shorter wavelength in order to obtain an emission closer to 576 nm, obtained after SHG, as desired for retinal photocoagulation. This is achieved by aligning the *Ng* axis of the *Np*-cut crystal parallel to the fundamental beam's polarization. The 10 mm long crystal had highly transmissive AR coatings at the entrance and exit facets, with less than 0.01% reflectivity at 1053 nm and less than 0.2% reflectivity at 1147 nm. For SHG conversion, a type 1 LBO (lithium triborate) crystal ($\Theta = 90$, $\Phi = 0$) with dimensions $4 \times 4 \times 8.25\ mm^3$ (Castech Inc.) was used with AR coating on both facets of less than 0.1% reflectivity at 1053 nm and 1147 nm and less than 0.2% reflectivity at 573 nm.

For the cavity configuration, a highly reflective (HR) concave mirror with a radius of curvature 7.5 cm (M1) and a flat output coupler (M2) with 15% transmission at 1053 nm were used. M1 was positioned at 8 mm from the Nd:YLF crystal, and the overall cavity length was kept at approximately 70 mm. Without the Raman and the SHG crystals, a maximum peak output power 77 W was achieved at 1053 nm for 125 W of incident pump power, with a resultant slope efficiency and optical efficiency of 61% (Fig. 2). The output beam was always Gaussian transversal mode in the vertical direction, whereas the horizontal transversal mode changed gradually from a Gaussian mode (observed up to 10 W of pump power) to higher order transversal modes. At the maximum pump power of 125 W, the highest order transversal mode observed was TEM_{40}, corresponding to a maximum beam quality factor M^2 of approximately nine in the horizontal direction. By slightly shifting the location of the TIR of the resonant beam laterally with respect to the pump beam's line focus, it was possible to favor transverse TEM_{00} mode oscillation. Therefore, at the expense of efficiency, a second, smaller slope efficiency of 38% could be achieved for transverse fundamental mode (TEM_{00}) operation. It should be noted that for the purpose of retinal photo cauterization, a certain degree of multimode output is beneficial in order to generate homogeneous burn spots on the retina.

With the KGW placed inside the cavity and changing the output mirror M2 to an HR output coupler at 1053 nm with 0.7% transmission at 1147 nm and 2% transmission at 1163 nm, Raman laser emission was observed at the shorter wavelength. The KGW crystal was placed closely to the beam waist located at the output coupler where the beam diameter is approximately 100 μm, as calculated using LASCAD software. Even after recoating at the factory (Castech Inc.), damage to the AR coating at the crystal's facets was the limiting factor for the maximum pump power, which had to be kept below 70 W. A slope efficiency of 21% and optical efficiency of 18% were achieved at 1147 nm with 11.7 W of peak output power. Threshold pump power for the first Stokes emission was approximately 7 W. Laser emission at the unwanted wavelength of 1163 nm was not

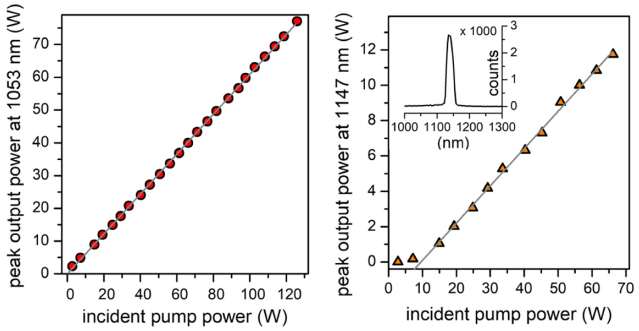

Fig. 2. Peak output power as a function of pump power at the fundamental wavelength (left) and the first Stokes wavelength of 1147 nm (right). Inset: emission wavelength measured at maximum pump power showing a single emission at 1147 nm.

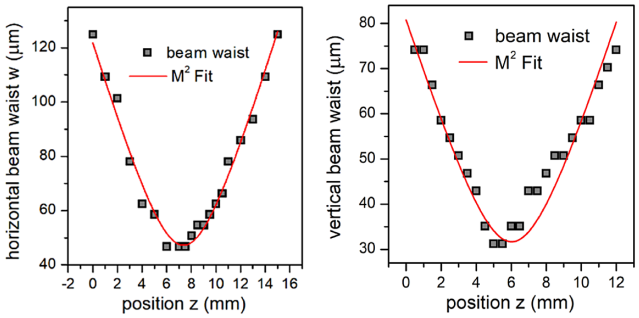

Fig. 3. M^2 measurement in the horizontal direction (left) of the 1147 nm output beam showing a beam quality factor of 2 and for the vertical direction (right) showing a beam quality factor of 1.1.

observed due to the higher transmission of the output coupler at this wavelength (see inset Fig. 2). The M^2 quality factors in the vertical and horizontal directions, measured at 66 W of pump power, were 1.1 and 2, respectively, as shown in Fig. 3. The much better beam quality of the Stokes beam with respect to the fundamental laser beam is expected due to the Raman cleanup effect.

After insertion of the LBO frequency doubling crystal, the output coupler was changed to a high-reflectivity mirror at the fundamental and first Stokes wavelength for operation at the frequency-doubled wavelength of 573.5 nm (Fig. 4). Operating temperature of the LBO was 63 deg Celsius, maintained by a temperature-controlled copper heat sink. The LBO crystal had to be inserted in the middle of the cavity (see Fig. 1) in order to maintain the efficiency of the Raman crystal that needed to be placed at the cavity's beam waist, closest to the output coupler.

As the Raman crystal was not optimized for transmission of the yellow wavelength, we measured the transmission of the KGW crystal together with the output coupler at 573 nm with the help of an OPO. A transmission value of 50.3% was measured at 573 nm. The maximum pump power had to be further limited to 50 W in order to avoid damage to the LBO crystal. At this pump power, the transmission corrected maximum yellow output power at 573 nm was 6 W. The corresponding slope efficiency was 12% with a just marginally smaller optical efficiency. A comparison of the fundamental (1053 nm), Raman (1147 nm), and SHG (573 nm) output power at the highest pump powers is shown in Fig. 4, where an efficient conversion

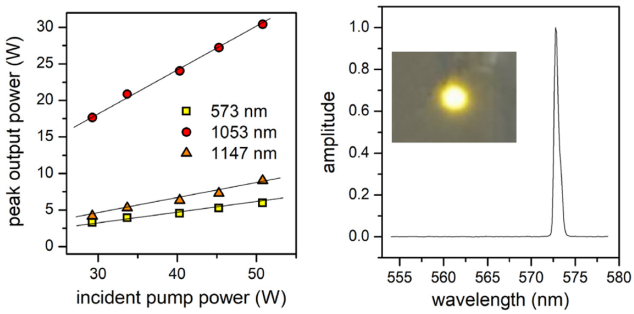

Fig. 4. Comparison of laser peak output power results at close to maximum pump powers (left) and spectrum of the yellow laser with inset of a picture of the laser beam (right).

from the first Stokes wavelength to the yellow emission can be observed.

VBG equipped diodes are very sensitive to changes in temperature, duty cycle, diode current, and pulse duration. Therefore, the desired effect of linewidth narrowing could only be achieved under strict maintenance of 5 Hz repetition rate and 350 μs pulse duration, decreasing the diode's Peltier temperature gradually from initially 33 deg Celsius down to 27 deg Celsius upon increasing diode current up to 140A [18]. However, higher pulse rates (5%) and durations (500 μs) are possible with standard VBG equipped diodes [21]. One highly recommended and, nowadays, commonly used pulsed regime for retinal photo cauterization is the subthermalmicropulse mode (SDM), thought to limit the amount of damage to subadjacent tissue. This mode uses micropulses during 200 ms with approximately 100 μs pulse duration and approximately 2 ms pulse interval [22]. The peak power for SDM is approximately 25%–50% of the power required for a visible threshold burn of the retina, which, for comparison, corresponds to a laser wavelength of 810 nm, a burn spot size of 200 μm diameter, and an approximately 6 W at 5% duty cycle [23]. However, as discussed previously, the absorption at 573 nm is much more adequate in terms of tissue absorption and has a several times higher cross section than at 810 nm. This latter effect should permit the simultaneous formation of several laser burn spots (grid photocoagulation [24]) with our available peak output power. Therefore, our results could be easily applied to SDM operating mode in retinal photo cauterization, using diodes equipped with VBG. Finally, wavelengths close to 573.5 nm can be achieved by frequency doubling of either directly emitting ytterbium(Yb)-doped lasers or combined Yb-Raman lasers and by Raman conversion of Q-switched 532 nm lasers in chemical vapor deposition (CVD)-diamond [25–27]. However, these methods are more complex and less cost efficient than the setup proposed in this work, and it is unclear if the necessary laser parameters for SDM can be achieved.

To our knowledge, a side-pumped Nd:YLF/KGW and frequency-doubled Raman laser producing 11.7 W of output power at 1147 nm with 21% of slope efficiency and 6 W of output power at 573 nm with 12% slope efficiency has been shown for the first time. Particularly, the slope efficiency and output power demonstrated for the first Stokes wavelength are higher than what has been achieved so far, even when compared to longitudinally pumped setups and oxide fundamental crystals. The yellow wavelength of 573.5 nm is, to our knowledge, the closest to the optimum wavelength of 576 nm achieved with an intracavity-converted Raman laser. The VBG diode-side-pumped configuration permits cost efficiency, less complexity in terms of size and cavity components, and good beam quality with high slope efficiency.

Funding. Science Foundation of the State of São Paulo FAPESP (2017 10765-5).

Acknowledgment. We would like to thank Dr. Helen Pask from Macquarie University for helping us with the recoating of our crystals and Dr. Jessica Dipold for help with the paper.

Disclosures. The authors declare no conflicts of interest.

REFERENCES

1. X. Yang, O. Kitzler, D. J. Spence, Z. Bai, Y. Feng, and R. P. Mildren, Opt. Lett. **45**, 1898 (2020).
2. H. M. Kretschmann, F. Heine, G. Huber, and T. Halldórsson, Opt. Lett. **22**, 1461 (1997).
3. V. Kapoor, V. Karpov, C. Linton, F. V. Subach, V. V. Verkhusha, and W. G. Telford, Cytometry A **73**, 570 (2008).
4. V. Kapoor, F. V. Subach, V. G. Kozlov, A. Grudinin, V. V. Verkhusha, and W. G. Telford, Nat. Methods **4**, 678 (2007).
5. N. S. Kapany, N. A. Peppers, H. C. Zweng, and M. Flocks, Nature **199**, 146 (1963).
6. J. H. Lock and K. C. Fong, Med. J. Malaysia **65**, 88 (2010).
7. W. G. Zijlstra, A. Buursma, and W. P. Meeuwsen-Van der Roest, Clin. Chem. **37**, 1633 (1991).
8. H. Zhu, Y. Duan, G. Zhang, C. Huang, Y. Wei, H. Shen, Y. Zheng, L. Huang, and Z. Chen, Opt. Express **17**, 21544 (2009).
9. P. Dekker, H. M. Pask, D. J. Spence, and J. A. Piper, Opt. Express **15**, 7038 (2007).
10. J. Lee, H. M. Pask, P. Dekker, and J. A. Piper, Opt. Express **16**, 21958 (2008).
11. X. Li, H. M. Pask, A. J. Lee, Y. Huo, J. A. Piper, and D. J. Spence, Opt. Express **19**, 25623 (2011).
12. A. J. Lee, D. J. Spence, J. A. Piper, and H. M. Pask, Opt. Express **18**, 20013 (2010).
13. Y. Lü, X. Zhang, S. Li, J. Xia, W. Cheng, and Z. Xiong, Opt. Lett. **35**, 2964 (2010).
14. M. Pollnau, P. J. Hardman, M. A. Kern, W. A. Clarkson, and D. C. Hanna, Phys. Rev. B **58**, 16076 (1998).
15. V. G. Savitski, I. Friel, J. E. Hastie, M. D. Dawson, D. Burns, and A. J. Kemp, IEEE J. Quantum Electron. **48**, 328 (2012).
16. Y. K. Bu, C. Q. Tan, and N. Chen, Laser Phys. Lett. **8**, 439 (2011).
17. J. J. Neto, J. Lin, N. Wetter, and H. M. Pask, Opt. Express **20**, 9841 (2012).
18. N. U. Wetter and A. M. Deana, Opt. Express **23**, 9379 (2015).
19. C. C. Kores, J. J. Neto, D. Geskus, H. M. Pask, and N. U. Wetter, Opt. Lett. **40**, 3524 (2015).
20. A. A. Kaminskii, K. Ueda, H. J. Eichler, Y. Kuwano, H. Kouta, S. N. Bagaev, T. H. Chyba, J. C. Barnes, G. M. A. Gad, T. Murai, and J. Lu, Opt. Commun. **194**, 201 (2001).
21. R. H. Page, R. J. Beach, V. K. Kanz, and W. F. Krupke, Opt. Lett. **31**, 353 (2006).
22. J. Li and Y. M. Paulus, Int. J. Ophthal. Res. **4**, 259 (2018).
23. G. Dorin, Semin. Ophthalmol. **18**, 147 (2003).
24. D. Lavinsky, J. A. Cardillo, L. A. S. Melo, Jr., A. Dare, M. E. Farah, and R. Belfort, Jr., Ophthalmol. Vis. Sci. **52**, 4314 (2011).
25. M. Jacquemet, E. Goyat, A. Mugnier, and D. Pureur, Proc. SPIE **7195**, 71950G (2009).
26. E. E. Rowen, G. Vashdi, J. Lasri, and E. Inbar, Proc. SPIE **8961**, 89611P (2014).
27. R. P. Mildren, J. E. Butler, and J. R. Rabeau, Opt. Express **16**, 18950 (2008).